Available online at www.sciencedirect.com
ScienceDirect
Journal of Nuclear Materials 358 (2006) 26–34
journal of nuclear materials
www.elsevier.com/locate/jnucmat

Changes in hardness and elasticity of a Ti_6Al_4V alloy under helium irradiation

S.H. Chen [a,*], G. Schumacher [b], Z.Y. Xu [c], M. Richter [d]

[a] College of Materials and Chemistry and Chemical Engineering, Chengdu University of Technology, 610059 Chengdu, PR China
[b] Structure and Dynamics of Solids, Hahn-Meitne-Institut Berlin GmbH, Glienicker Strasse 100, 14109 Berlin, Germany
[c] Southwestern Institute of Physics, 610041 Chengdu, PR China
[d] Forschungszentrum Rossendorf, P.O. Box 510119, 01314 Dresden, Germany

Received 6 March 2006; accepted 23 June 2006

Abstract

Ti_6Al_4V specimens have been irradiated at different temperatures with 200 keV He ions. Microhardness and elastic modulus of the unirradiated and irradiated specimens were measured by means of the nano-indentation technique and analyzed using the Oliver–Pharr method. The indentation depth of all samples is 700 nm, which is comparable in magnitude to the ion range. The subsurface structure of the Ti_6Al_4V specimens was investigated by the X-ray diffraction technique. The measurements indicate that the microhardness increased with the irradiation temperature from room temperature to 600 °C while the elastic modulus almost monotonically decreased. The Irradiation at 700 °C, however, caused softening and slight increase of the elastic modulus within the surface layer of the specimens. The hardening and reduction of the elastic modulus of the Ti_6Al_4V alloy under irradiation conditions used in this study is tentatively explained by a model based on the presence of point defects and dispersed obstacles of β-precipitates. The softening and slight increase of elastic modulus of helium-irradiated Ti_6Al_4V at 700 °C might be related to the coarsening of β-precipitates and formation of the hybrid γ-TiH phase in α-phase.

1. Introduction

Titanium alloys are being considered as structural materials for fusion reactor applications [1–3]. Among the reasons for their selection are the high strength-to-weight ratio, high electrical resistivity, good mechanical and thermal properties and exceptional corrosion resistance. Moreover, they have low swelling tendency under a wide variety of irradiation conditions and fast induced radioactive decay (>10 years after shutdown after V and Cr, Ti exhibits the third fastest decay rate), compatibility with coolants such as helium and water [4,5]. The latest design of the next fusion reactor includes the use of titanium alloys in specific parts of the structure. In particular, the $(\alpha + \beta)$ alloy Ti_6Al_4V has been proposed to be used in flexible supports between the ITER blanket modules and the vacuum vessel [6,7].

* Corresponding author. Tel.: +86 28 84079015; fax: +86 28 84079074.
E-mail address: chensh@cdut.edu.cn (S.H. Chen).

0022-3115/$ - see front matter © 2006 Elsevier B.V. All rights reserved.
doi:10.1016/j.jnucmat.2006.06.009

One of the most important technical issues for the titanium alloys as fusion structural material is the influence of the transmutant helium production on the irradiation-related mechanical property changes. Until now, there are limited data available on the irradiation behavior of these materials. For example, Rodchenkov et al. [8] irradiated an $(\alpha+\beta)Ti_6Al_4V$ alloy with neutrons up to a dose of 0.35–0.42 dpa at temperatures between 240 and 260 °C. They showed that irradiation to a dose level of about 0.4 dpa resulted in changes of the mechanical properties of the Ti_6Al_4V alloy. The effects of irradiation depend on test temperature and material structure. At 20 °C the radiation hardening was less significant than that at 260 °C. The irradiation caused significant reduction in fracture toughness of the Ti_6Al_4V alloy and a slight decrease of low cycle fatigue in the range of large strain amplitudes. The mechanical properties (tensile, fracture toughness and fatigue) change differently due to irradiation of the different material structures. For the simulation of the fusion neutrons, Marmy and Leguey [9] have carried out the tensile and fatigue performance of a two-phase $(\alpha+\beta)Ti_6Al_4V$ alloy and a α-$Ti_5Al_{2.5}Sn$ alloy using 590 MeV protons. They showed that the unirradiated tensile performance of both alloys is roughly identical. However, irradiation hardening is much stronger in the $(\alpha+\beta)Ti_6Al_4V$ alloy compared to the α-alloy, and the ductility is correspondingly strongly reduced. The fatigue resistance of the $Ti_5Al_{2.5}Sn$ alloy is slightly better than that of the Ti_6Al_4V alloy. Irradiation did not significantly affect the fatigue performance of both alloys, except for high-imposed strains, where a life reduction was observed in the case of the Ti_6Al_4V alloy. Higashiguchi and Kayano [2] irradiated pure titanium with fast neutrons to fluences up to 3×10^{19} n/cm^2 and at a temperature below 150 °C. Their tensile tests were carried out at temperatures between that of liquid nitrogen and 135 °C. They showed that the ductility at liquid nitrogen temperature was enhanced by irradiation and did not decrease significantly at the higher test temperatures. The corresponding hardening increased up to 100% of the initial flow stress of the relatively soft titanium studied. Kohyama et al. [10] irradiated pure Ti and Ti_6Al_4V with neutrons at fluences up to 5×10^{20} n/cm^2 at 260 °C. They observed in pure Ti a saturation of hardening at a fluence of 1.2×10^{20} n/cm^2, and a hardening of approximately 35% of the initial flow stress. No saturation of hardening was observed in the Ti_6Al_4V alloy and the irradiation hardening and corresponding loss of ductility were more significant than in pure Ti.

Even though Ti_6Al_4V has been thoroughly studied and used in a number of large structures, it has not been used in fusion components and requires additional research before large prototypical components can be fabricated. There is also a lack of information on the mechanical properties of the helium irradiated titanium alloys at higher temperatures. In this work, a candidate $(\alpha+\beta)Ti_6Al_4V$ alloy has been irradiated with 200 keV helium ions at room temperature and between 400 and 700 °C. Due to the small range of helium ions of about 700 nm only a very thin subsurface layer less than 1 μm is affected by irradiation. Changes in hardness and elasticity in this subsurface layer under ionirradiation were therefore measured by means of the nano-indentation technique.

This paper describes the helium irradiation effects on the nano-indentation properties of an $(\alpha+\beta)Ti_6Al_4V$ alloy, with the objective of assessing embrittlement of the helium irradiated titanium alloy at different temperatures. Grazing incidence X-ray diffraction (GIXRD) and laser scanning confocal microscopy (LSCM) were undertaken and were related to the observed changes in the mechanical properties.

2. Experimental details

2.1. Materials, specimens and irradiation parameters

The Ti_6Al_4V samples were provided by AAB Company, which has a duplex structure composed of equiaxed primary α-grains of about 4–10 μm size, together with colonies of elongated secondary α-grains of $\approx$0.5 μm width and 3 μm length. They are surrounded by the intergranular β-phase. The total content of β-phase was estimated to be about 9 vol.%.

Prior to helium irradiation, all the Ti_6Al_4V specimens were mechanically polished using increasingly finer polishing material. Final polishing was done with diamond paste. The specimen size was 10 mm × 10 mm. Implantation of 200 keV He ions was done at different temperatures between RT and 700 °C at FZ Rossendorf, Germany. The mean ion flux was 1×10^{17}/cm^2 and the irradiation temperatures were room temperature, 400 °C, 500 °C, 600 °C and 700 °C. The depth profiles of damage

and helium ions were calculated using the TRIM 85 code [11]. The damage peak and stopped-ion peak were at about 700 nm below the surface.

2.2. Indentation and hardness profiling

Nano-indentation is one of the few characterization methods by which the surface mechanical property can be evaluated without interference of bulk material characteristic [12]. Two mechanical properties most frequently evaluated from load and depths of indenter penetration are the elastic modulus, E, and the hardness, H, which are calculated by the following equations [13]:

$$H = \frac{P_{\max}}{A_c}, \tag{1}$$

$$\frac{1}{E_{\text{eff}}} = \frac{1-v^2}{E} + \frac{1-v_i^2}{E_i}. \tag{2}$$

In Eq. (1), the parameter $P_{\max}$ and A_c represents the peak load and the projected contact area between the indenter and specimen, respectively. The term v, v_i in Eq. (2) is Poisson's ratio of the specimen and the indenter respectively, and E_i is the elastic modulus of the indenter. E_{eff} is linked to A_c and the unloading stiffness S of the specimen by the following relation:

$$E_{\text{eff}} = \frac{\sqrt{\pi}}{2}\frac{S}{\sqrt{A_c}}. \tag{3}$$

In this work, the nano-indentation hardness was measured in an instrumented nano-indenter (CSEM, Switzerland) having a Berkovich type diamond tip with a face angle of 142.38°. Before the experiments, the indenter shape was calibrated by a standard indentation procedure in fused silica between 0.1 and 100 mN. To reduce the point-to-point data scatter because of probable influences of inhomogeneous dislocation microstructure, crystallographic orientation and anisotropic microstructures, 14 penetration depths between 50 nm and 700 nm were chosen and 15 measurements were repeated at each depth in a direction normal to the irradiated surface of each sample. Therefore, 210 data were obtained for each sample. At each test, the loading speed was adjusted to keep 30 s loading time, 2 s delay at peak load and 30 s unloading time. An improved version of the Pharr technique [14] was used to minimize statistical errors.

2.3. XRD analysis of surface layers

By employing a fixed low angle of incidence, the GIXRD technique allows the depth of penetration of the X-rays to be localized to the extreme surface of the sample. GIXRD is therefore ideal for specimens with shallow modified layers. In this work, the thin layers of all the Ti_6Al_4V specimens were characterized using GIXRD (X'Pert Pro MPD, Philips, Netherlands) in the $\omega/2\theta$ mode where the grazing angle ω was 1° and the range of 2θ varied between 30° and 80°. The voltage and anode current used were 40 kV and 40 mA, respectively. CuKα-radiation ($\lambda = 0.15405$ nm) and continuous scanning mode with 0.02 rad of interval and 0.25 s of set time were used to collect the GIXRD patterns of the samples. Further, parallel X-ray incident beams of hybrid mirror with a divergence slit of 1/8° and diffracted beam of the parallel plate collimator with Soller slit 0.04 rad and prepositional detector were used in all GIXRD experiments.

2.4. Surface roughness measurements

A number of the inherent features of LSCM, such as high resolution close to the theoretical limit for optical systems, large effective depth of field, no vacuum requirement and its ability to quantify surface topography down to a few tens of nano-meters, make the technique ideally suited to characterization of surface roughness [15]. Therefore, to observe the effect of helium irradiation at different temperatures on the surface morphologies, the surfaces of helium irradiated Ti_6Al_4V were imaged by LSCM (Olympus-OLS-1100) and the surface roughness of these samples was also measured by LSCM.

3. Results

3.1. Changes in hardness and elasticity

The typical load–depth curves of Ti_6Al_4V unirradiated and irradiated at different temperatures are plotted in Fig. 1. The variations of the residual indentation depths show their distinctions in the material's ability against deformation or the hardness. On the load–depth curves, although the unloading slope of all the Ti_6Al_4V samples are approximately the same, the recovery depth of the unirradiated Ti_6Al_4V sample is relatively small, which suggests that the unirradiated Ti_6Al_4V alloy has the largest contact stiffness and elastic modulus.

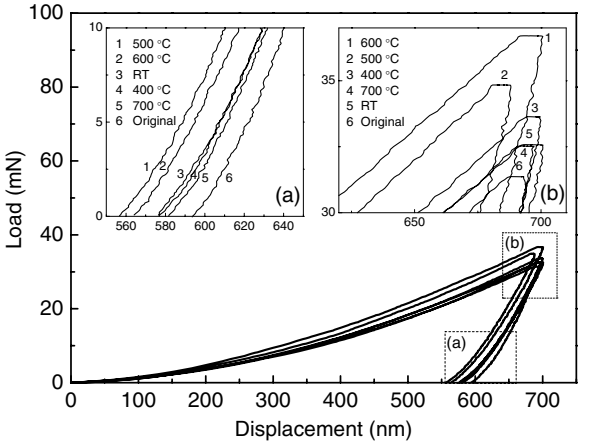

Fig. 1. Comparison of indentation force versus indentation depth curves for various Ti_6Al_4V samples in the unirradiated original condition and after irradiation at room temperature, 400 °C, 500 °C, 600 °C and 700 °C. The indentation depth of all samples is 700 nm. The insets (a) and (b) are the enlarged part of corresponding (a) and (b) in the indentation depth curves, showing recovery depths of the samples and their loading responses at maximum load, respectively.

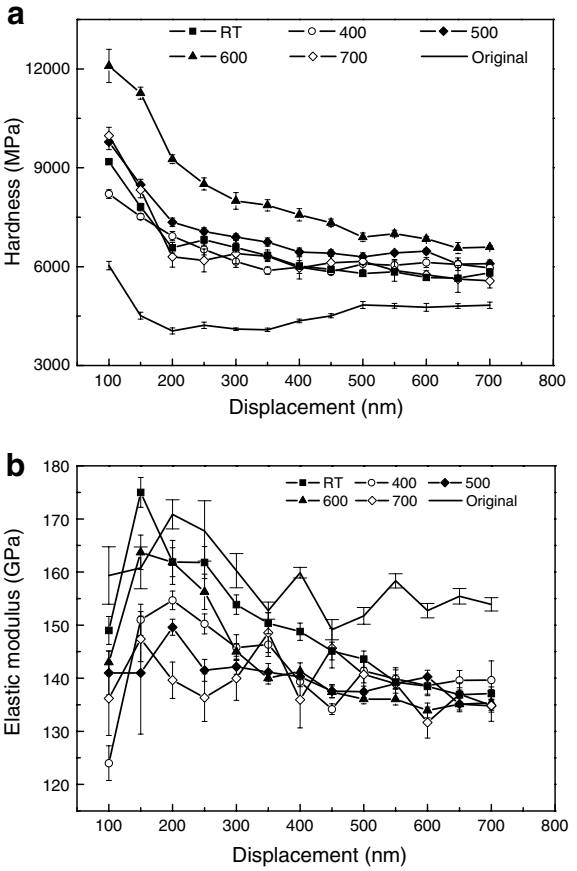

Fig. 2. Hardness (a) and elastic modulus (b) of Ti_6Al_4V samples unirradiated (original Ti_6Al_4V) and irradiated at room temperature, 400 °C, 500 °C, 600 °C and 700 °C, as a function of indentation depth between 100 nm and 700 nm, respectively. The continuous line is placed to guide the eyes through the experimental points.

As shown in Fig. 2(a), the load dependence of nano-indentation hardness H for various samples is different. Clearly, the samples irradiated at 600 °C experienced a strong hardening and showed the highest hardness at all displacements compared to the samples irradiated at other temperatures, namely from 12.1 GPa at a displacement of 100 nm to 6.6 GPa at 700 nm. The hardness value of the samples irradiated at 500 °C is lower than that of the sample irradiated at 600 °C, but higher than that of the sample irradiated at room temperature and 400 °C at almost all displacements, although it is difficult to compare the measured hardness values of the samples irradiated at room temperature and 400 °C because of the fluctuation of the hardness data in the depth range between 100 nm and 700 nm. However, after irradiation at 700 °C, the nano-hardness reduced sharply to the hardness value irradiated at room temperature and 400 °C. The hardness values of all irradiated specimens are always larger than the hardness of the unirradiated samples (≈4.7 GPa). It is worth noting that a more stable plateau in nano-hardness and Young's modulus were obtained after the first 500 nm indentation depth, as shown in Fig. 2(a). In comparison with the nano-hardness measurements in Fig. 2(a), where the maximum values occurred at a depth of 100 nm, the elastic modulus of all the samples reached its maximum between 150 nm and 200 nm, as shown in Fig. 2(b), where the elastic moduli of Ti_6Al_4V samples irradiated at various temperatures are plotted. In Fig. 2(b), the hardness values of all the specimens at the depth of 50 nm are omitted, since the scattering of the data is too large at such small indentation depth due to the increasing influence of surface effects, e.g., of the surface roughness.

3.2. XRD and GIXRD measurements

Fig. 3(a) shows the GIXRD patterns of Ti_6Al_4V specimens both in the unirradiated condition and after irradiation at different temperatures. The β-Ti phase could not be detected in the unirradiated specimens. This might be due to an insufficient volume amount of the β-Ti phase in the sample surface. The amount of β-phase increased after irradiation at

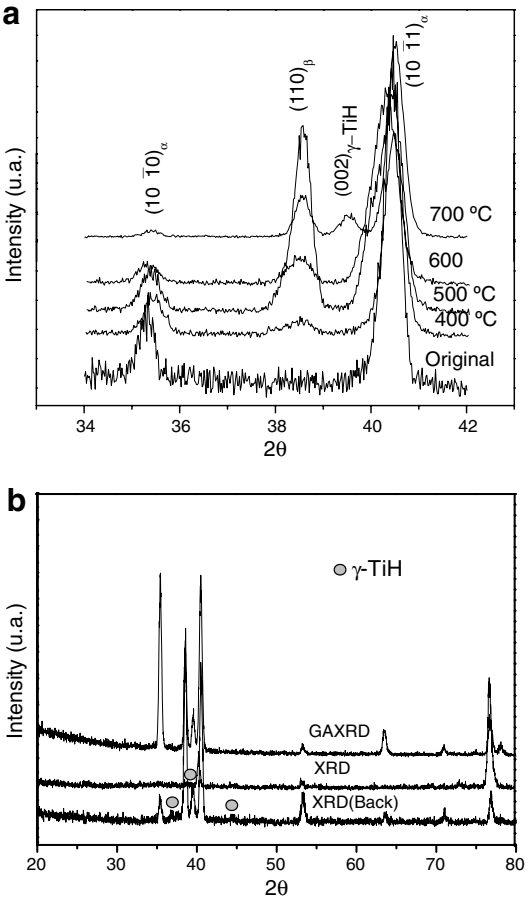

Fig. 3. GIXRD patterns of Ti_6Al_4V specimens unirradiated and irradiated at different temperatures (a) and comparison of GIXRD and XRD patterns from the irradiated surface and XRD pattern from the backside of the Ti_6Al_4V specimen irradiated at 700 °C (b).

higher temperatures, permitting the β-phase to be measured by GIXRD (Radiation-enhanced diffusion might stimulate the precipitation of the β-phase [9,16]). In comparison to the β-Ti peak of the samples irradiated at temperatures lower than 700 °C, the width of the β-Ti peak of the sample irradiated at 700 °C also decreased indicating an increase of the grain size of the β-phase.

A further striking result in Fig. 3(a) is the presence of an additional diffraction peak at $2\theta = 39.5°$ after irradiation at 700 °C. This peak indicates that a new phase existed in the irradiated Ti_6Al_4V sample at 700 °C. However, it is difficult to identify this new phase, since no other new strong peaks are observed. Another question is if this new phase resulted from helium irradiation at 700 °C or not. The normal θ–2θ XRD patterns of all the unirradiated and irradiated specimens were therefore recorded at both sides of all the irradiated samples. The results showed that the additional 39.5° diffraction peak was only observed on the sample irradiated at 700 °C (Fig. 3(b)). However, for the unirradiated side of the sample irradiated at 700 °C, except the diffraction peak at 39.5°, the other two peaks at 36.9° and 44.6° were also relatively strong (Fig. 3(b)). These peaks are corresponding to the reflection (0 0 2), (1 1 1) and (2 0 0) of γ-TiH phase, respectively. A comparison of the XRD and GIXRD patterns in Fig. 3(a) and (b) showed clearly that the occurrence of this γ-TiH phase was a direct result of heat treatment effect and may not related to the helium irradiation at this temperature.

3.3. Changes in surface roughness

Fig. 4 shows typical images of the specimens after irradiation at different temperatures. It can be seen that there are many flakes on all the irradiated samples and we ascribe them to helium bubbles on the sample surface [17]. The extent of blistering resulting mainly from helium bubbles formation after irradiation from room temperature to 600 °C is similar. The quantitative measurements have shown that the average surface roughness of the specimens after irradiation at room temperature, 400 °C, 500 °C, 600 °C and 700 °C are 0.3381 μm, 0.5960 μm, 0.5035 μm, 0.6210 μm, 0.9582 μm, respectively. Therefore, the surface roughness of the Ti_6Al_4V specimen increases severely when the irradiation temperature is increased from 600 °C to 700 °C. Further, the surface morphology of the sample irradiated at 700 °C is quite different from that of the samples irradiated at other temperatures and may be an indication of the formation of γ-TiH phase.

4. Discussion

The hardness of the unirradiated Ti_6Al_4V samples decreases with the increase of the indentation depth (see Fig. 2(a)). This kind of depth effect is usually called the indentation size effect [13]. The strain-hardening effect was usually used to explain the increase of hardness with strain [18,19]. However, for sharp Berkovich indenter (with a curvature radius of ≈150 nm) and large indentation depth, the representative strain is only determined by the face angle of indenter and independent of the indentation load. This should result in a constant hardness at various depths. Nevertheless, some possible explanations

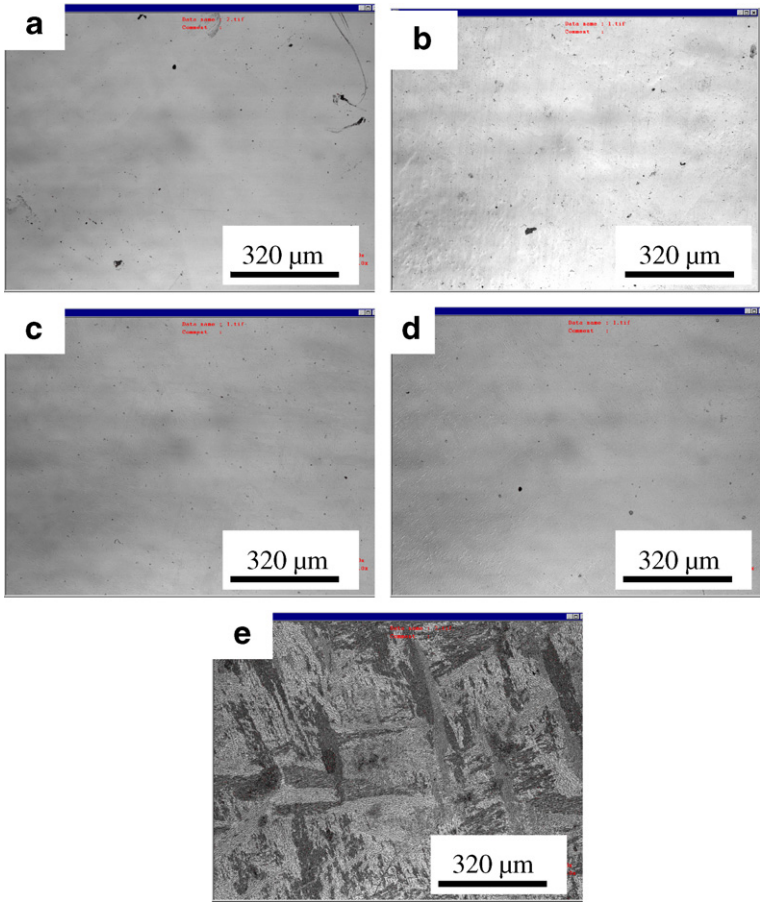

Fig. 4. LSCM projections of Ti_6Al_4V surfaces after irradiation at: (a) room temperature; (b) 400 °C ; (c) 500 °C ; (d) 600 °C and (e) 700 °C.

on the indentation size effect are reported in the literature. By applying the strain gradient plasticity theory in indentation, Nix and Gao [20] pointed out that the geometrically necessary dislocations could increase the effective yield stress of the material. The dislocation density increases with the decrease of the indentation depth, resulting in the indentation size effect. Froehlich et al. [21] indicated that hardness is in fact the energy per volume of plastic deformation, including volume deformation energy and free surface energy. The free surface area of indentation grows up with depth to cause the indentation size effect. Due to the complex microstructure of the materials and the different deformation mechanisms (elastic and plastic) during the indentation process, the indentation size effect is still far from being entirely understood.

All curves of irradiated samples in Fig. 2(a) show a monotonic decay of hardness as a function of the indentation depth, which may result in a fairly complicated situation due to contributions by at least three kinds of layers, i.e., the surface layer where the surface effect and the displacement effect dominate, the second layer where the displacement and the helium deposition are effective, and the substrate which is free from irradiation effects. The hardness data for the specimen irradiated at 700 °C are less reliable compared to the others because of insufficient surface finishing as shown in Fig. 4. For the given irradiation condition, the hardness peak appears at about 100 nm depth near the surface. The reason for the occurrence of this peak is not quite clear, although a hardness peak at about the same depth is also reported in the literature for Si, NiTi and He^{+}–Ni^{3+} dual-ion irradiated Fe–Cr–2W steel [22,23].

The creation of the γ-TiH phase under 200 keV helium irradiation at 700 °C is an astonishing result, since the Ti_6Al_4V samples are helium-irradiated under high vacuum conditions. However, it is demonstrated that titanium has a strong chemical affinity and can absorb and store large amounts of

hydrogen [24–26], which causes embrittlement of the material. By using backscattering spectrometry, nuclear reaction analysis (NRA) and heavy ion elastic recoil detection analysis (HERDA), Schmidt et al. [27] and Soltani-Farshi et al. [28,29] have examined the hydrogen content of the boron-, carbon-, nitrogen-, fluorine- and neon-implanted titanium and Ti_6Al_4V alloy at room temperature, and found a correlation between phase formation and accumulated hydrogen. A significant hydrogen accumulation (up to 30 at.% for carbon-implanted titanium) was observed in the implanted layer measured by NRA. At B-, C- and N-concentrations above 30 at.%, the hydrogen content decreases with increasing phase precipitation and reaches a value of less than 0.6 at.% in the formed boride, carbide and nitride layer. No noticeable hydrogen effect was observed for oxygen and fluorine-implanted titanium. These authors believed that ion implantation into pure titanium and titanium base alloys will lead to the distortion of the lattice causing the hydrogen to diffuse into the implantation region and can thus affect the formation of defects, vacancies and other phases. However, in our work, it seems that the content of accumulated hydrogen depends mainly on the irradiation temperature, since the formation of the γ-TiH phase was only detectable by XRD in the helium-implanted sample at 700 °C. At lower irradiation temperatures, the formation of the γ-TiH phase was not observed, which is consistent with the results reported in the literature [30]. Further transmission electron microscopy (TEM) experiments and other analyses are in progress to better understand the formation of the γ-TiH phase in the Ti_6Al_4V samples under ion implantation.

Hardening produced by irradiation depends on the type and energy of the irradiation particle and also on the structure and chemical composition of the material irradiated. The behavior of the Ti_6Al_4V alloy is controlled by the irradiation response of its main component, the α-phase. An attempt to compile the changes in the average nano-hardness and elastic modulus between 500 nm and 700 nm of all the Ti_6Al_4V samples as a function of irradiation temperatures is made in Fig. 5(a) and (b). From these figures, it is concluded that helium irradiation at a temperature lower than 600 °C will lead to the continuous increase of the hardness and the decrease of the elastic modulus. A very significant enhancement of helium irradiation hardening, i.e., a hardening peak, has occurred at 600 °C. At around 700 °C hardening is no longer observed. Comparable

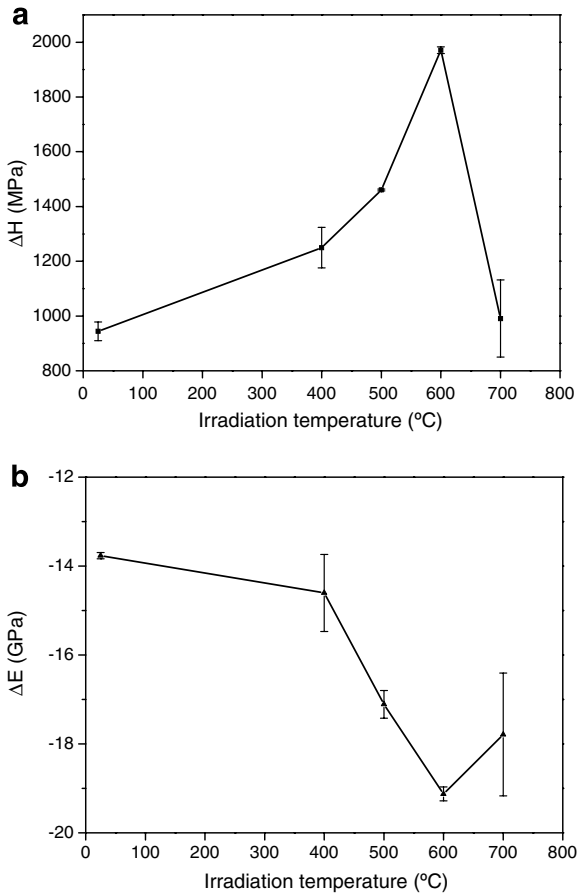

Fig. 5. Changes in nano-indentation hardness (a) and elastic modulus (b) of Ti_6Al_4V specimens subjected to helium irradiation at room temperature, 400 °C, 500 °C, 600 °C and 700 °C. The values of ΔH and ΔE correspond to the difference in hardness values and elastic modulus of irradiated and unirradiated specimens for the indent depth range from 500 nm to 700 nm, respectively.

changes were also observed in Fe–8–9Cr–2W martensitic steels under helium irradiation at 300–500 °C and corresponding recovery of dislocation structure in the near surface layer, typically to a depth of ≈500 nm for the case of 500 °C irradiation was observed by transmission electron microscopy [31]. After irradiation with 9 MeV Al ions and neutron irradiation to a dose level of 2.1 and 32 dpa at temperatures between 450 °C and 700 °C, the presence of a β-precipitation in the Ti_6Al_4V alloy have also been demonstrated in literatures [10,32–36]. They showed that the precipitate size is inversely proportional to the irradiation temperature (between 65 and 400 nm) and the increased hardening is a direct consequence of the precipitation of the very fine β-precipitates in α-phase due to the presence

of vanadium. The cause of this precipitation was determined to be radiation-enhanced diffusion and radiation-induced segregation of the undersized β-stabilizing element, vanadium, to the defect clusters. In our study, helium is insoluble in metals and is considered as either trapped in single vacancies or precipitated into helium bubbles. Therefore, the microstructural defects that had been produced by helium irradiation could be small dislocation loops, vacancies and helium bubbles. The latter are expected to be produced preferentially at higher temperatures where helium atoms in the alloy are mobile. The β-phase precipitates serve as obstacles for the dislocations. Therefore, the observed irradiation hardening lower than 600 °C could be resulted from irradiation-induced β-phase precipitates, interstitial-type dislocation loops and implanted helium atoms. As shown in Fig. 3(a), the width of the β-phase peak of the sample irradiated at 700 °C is smaller than that of samples irradiated below 700 °C. Therefore, the size of β-phase precipitates may become larger after irradiation at 700 °C. Considering the fact that γ-TiH is with low strength and cleaves at stresses much lower than the parent alloy [30], the observed softening at 700 °C may result from coarsening of β-phase precipitates and from the soft γ-TiH phase.

The elastic modulus is considered to be physically dependent on the interatomic bond strength, atomic spacing and bond density. Therefore, the modulus considered to decrease as irradiation-induced strain is reduced at high irradiation temperatures since the irradiation-induced defects are more stable during low-temperature irradiation and tend to self-anneal with increased irradiation temperature [37,38]. The observed trends in the elastic modulus (Fig. 5(b)) can be explained based on the reduction of point defects such as vacancies and helium bubbles from room temperature to 600 °C, and precipitation of the very fine β-precipitates in α-phase of the Ti_6Al_4V alloy. The slight increase of elastic modulus at 700 °C may also be resulted from coarsening of β-precipitates and from the soft γ-TiH phase in α-phase.

5. Conclusions

Ti_6Al_4V specimens have been irradiated at room temperature, 400 °C, 500 °C, 600 °C and 700 °C with 200 keV He ions. Microhardness and elastic modulus of the specimens unirradiated and irradiated at different temperatures were measured by means of nano-indentation technique and analyzed using the Oliver–Pharr method. The subsurface structure of the specimens was investigated by the GIXRD diffraction technique. The indentation depth of all samples is 700 nm, which is comparable in magnitude to the ion range. The measurements indicate that the microhardness increases and the elastic modulus decreases with the irradiation temperature from room temperature to 600 °C. Irradiation at 700 °C, however, caused softening and slight increase of elastic modulus within the surface layer of the specimens. The hardening and reduction of the elastic modulus of the Ti_6Al_4V alloy under the present irradiation conditions is tentatively explained by the presence of point defects and β-precipitates, which are dispersedly distributed and serve as obstacles for the interstitial-type dislocation loops. The softening and increase of elastic modulus of helium-irradiated Ti_6Al_4V at 700 °C might be related to the coarsening of β-precipitates and formation of the hybrid γ-TiH phase in α-phase.

Acknowledgements

The present work is partially funded by the Post-Doctoral Research Station in Science and Engineering of Southwestern Institute of Physics, the Key Science and Technology Program of Ministry of Education of China (No. 205139) and the High-Level Talented Returned Study-Abroad Scholars Program of Ministry of Personnel of China (Grant [2004] 61). The authors wish also to thank Professor Linmao Qian from the Tribology Research Institute, Southwest Jiaotong University and Dr Linghong Guo from the PANalytical XRD Application Research Laboratory, Analysis and Testing Center, Sichuan University for their help in nano-indentation experiments and GIXRD analyses as well as for the fruitful discussion.

References

[1] J. Davis, M.A. Ulrichson, R.A. Causey, J. Nucl. Mater. 212–215 (1994) 813.
[2] Y. Higashiguchi, H. Kayano, J. Nucl. Sci. Technol. 12 (1975) 320.
[3] G. Kalinin, V. Barabash, A. Cardella, J. Dietz, K. Ioki, R. Matera, R. Santoro, R. Tivey, T.I.H. Teams, J. Nucl. Mater. 283–287 (2000) 10.
[4] J.W. Davis, M.A. Ulrickson, R.A. Causey, J. Nucl. Mater. 212–215 (1994) 813.
[5] A. Hishinuma, J. Nucl. Mater. 239 (1996) 267.
[6] K. Ioki, V. Barabash, A. Cardella, F. Elio, Y. Gobar, G. Janeschitz, G. Johnson, G. Kalinin, D. Lousteau, M.

Onozuka, R. Parker, G. Sannazzaro, R. Tivey, J. Nucl. Mater. 258–263 (1998) 74.
[7] K. Ioki, V. Barabash, A. Cardella, F. Elio, H. Iida, G. Johnson, G. Kalinin, N. Miki, M. Onozuka, G. Sannazzaro, Y.U.M. Yamada, Fusion Eng. Des. 49&50 (2000) 467.
[8] B.S. Rodchenkov, A.V. Kozlov, Yu.G. Kuznetsov, G.M. Kalinin, Yu.S. Strebkov, J. Nucl. Mater. 307–311 (2002) 421.
[9] P. Marmy, T. Leguey, J. Nucl. Mater. 296 (2001) 155.
[10] A. Kohyama, K. Asano, N. Igata, J. Nucl. Mater. 141–143 (1986) 987.
[11] J.P. Ziegler, J.P. Biersack, U. LittmarkThe Stopping and Ranges of Ions in Materials, 1, Pergamon, New York, 1985.
[12] T. Wourgaurd, J.C. Dargenton, C. Thomas, V. Audurier, Surf. Coating Technol. 100 (1998) 103.
[13] W.C. Oliver, G.M. Pharr, J. Mater. Res. 7 (1992) 1564.
[14] A. Bolshakov, G.M. Pharr, J. Mater. Res. 13 (1998) 1049.
[15] D.N. Hanlon, I. Todd, E. Peekstok, W.M. Rainforth, S. Van der Zwaag, Wear 251 (2001) 1159.
[16] D.L. Plumton, G.L. Kulcinski, R.A. Dodd, J. Nucl. Mater. 144 (1987) 264.
[17] J. Yu, X. Zhao, W. Zhang, F. Chu, J. Nucl. Mater. 251 (1997) 150.
[18] Y.Y. Lc, M.M. Chaudhri, Phys. Status Solidi A, Appl. Res. 194 (2002) 19.
[19] M.M. Chaudhri, Acta Mater. 46 (1998) 3047.
[20] W.D. Nix, H. Gao, J. Mech. Phys. Solids 46 (1998) 411.
[21] F. Froehlich, P. Grau, W. Wrellmann, Phys. Status Solidi 42 (1977) 79.
[22] L. Qian, M. Li, Z. Zhou, H. Yang, X. Shi, Surf. Coatings Technol. 195 (2005) 264.
[23] Y. Katoh, H. Tanigawa, T. Muroga, T. Iwai, A. Kohyama, J. Nucl. Mater. 271&272 (1999) 115.
[24] B. Hoffmann, H. Baumann, F. Rauch, Nucl. Instrum. Meth. B 15 (1986) 361.
[25] B. Hoffmann, H. Baumann, F. Rauch, K. Bethge, Nucl. Instrum. Meth. B 36 (1989) 157.
[26] H. Baumann, Th. Lenz, F. Rauch, Mater. Sci. Eng. 69 (1985) 421.
[27] H. Schmidt, M. Soltani-Farshi, Mater. Sci. Eng. A 248 (1998) 73.
[28] M. Soltani-Farshi, H. Baumann, D. Rück, E. Richter, U. Kreissig, K. Bethge, Surf. Coatings Technol. 103&104 (1998) 299.
[29] M. Soltani-Farshi, H. Baumann, D. Rück, K. Bethge, Nucl. Instrum. Meth. B 127&128 (1997) 787.
[30] J.W. Davis, G.W. Wille, P. Heitzenroeder, J. Nucl. Mater. 233–237 (1996) 592.
[31] Y. Katoh, M. Ando, A. Kohyama, J. Nucl. Mater. 323 (2003) 251.
[32] O.A. Kojevnikov, S.A. Fabritsiev, Vopr. Atom. Nayki Techn.; Fis. Radiaz. Povr. Radiaz. Mater. 2 (1988) 1.
[33] S. Tähtinen, P. Moilanen, B.N. Singh, D.J. Edwards, J. Nucl. Mater. 307–311 (2002) 416.
[34] S.M.L. Sastry, J.E.O. Neal, in: H. Kimura, O. Izumi (Eds.), Titanium'80, Science and Technology, 1, The Metallurgical Society AIME, Warrendale, PA, 1980, p. 651.
[35] D.T. Peterson, in: H.R. Brager, J.S. Perrin (Eds.), Effect of Irradiation on Materials 11th International Symposium ASTM STP-782, American Society for Testing and Materials, Philadelphia, PA, 1982, p. 260.
[36] D.J. Edwards, B.N. Singh, P. Toft, in: Fusion Materials Semiannual Progress Report for the Period Ending June 30, 2000, DOE/ER-0313/28, p. 214.
[37] S. Nogami, A. Hasegawa, L.L. Snead, J. Nucl. Mater. 307–311 (2002) 1163.
[38] R. Blackstone, E.H. Voice, J. Nucl. Mater. 39 (1971) 319.